Multisine impedimetric probing of biocatalytic reactions for label-free detection of DEFB1 gene: How to verify that your dog is not human?

Pawel Niedzialkowski[1], Pawel Slepski[2], Joanna Wysocka[2], Joanna Chamier-Cieminska[3], Lukasz Burczyk[2], Michal Sobaszek[2], Anna Wcislo[1], Tadeusz Ossowski[1], Robert Bogdanowicz[2], Jacek Ryl[2,*]

[1] University of Gdansk, Wita Stwosza 63, 80-952 Gdansk, Poland
[2] Gdansk University of Technology, Narutowicza 11/12, 80-233 Gdansk, Poland
[3] Medical University of Gdansk, Debowa 23, 80-204 Gdansk, Poland
*Corresponding author: jacek.ryl@pg.edu.pl

Abstract

Albert is a dog (*Canis familiare simum*), but he does not realize this. Albert loves human food (and beer), watching movies on the internet, sleeping in bed, and more. But he should not do all these things. To convince him that, we have desinged a test procedure. The DEFB1 gene is unique to human species. Detecting its presence from saliva and in short periods may offer an advantage in the field of forensic medicine, and influence Albert's bad habits.

This study reveals novel utilization of the multisine impedance spectroscopy carried out during potentiodynamic polarization (pDEIS) of the electrode. We have utilized pDEIS to detect DEFB1 gene in collected saliva samples. The detection process was conducted at the boron-doped diamond surfaces functionalized with DEFB1-complimentary oligonucleotide sequence, anchored at the electrode surface. Next, a short-term electrode incubation in presence of target DNA sample allows for achieving DNA hybridization when exposed to human DNA material. The dsDNA orientation vs electrode surface is affected by polarization, and tracked by changes in the electrode kinetics preceded by subtle capacitance

dispersion effects. The optimized measurement conditions range between +0.5 and +0.9 V vs Ag|AgCl due to nonspecific DNA adsorption, affecting heterogeneous charge transfer. The DNA hybridization is not achieved in the case of non-complimentary ssDNA originated from any other species subjected to this test. The discussed differences obtained during electrode incubation are supported by the XPS analyses.

Keywords: beta-defensin 1 gene, impedance biosensor, boron-doped diamond, multisine impedance spectroscopy

1. Introduction

Many diseases can be easily diagnosed based on nucleic acid analyses, forming a rapid necessity to develop new techniques for DNA sequence detection, which is based on hybridization events [1]. The concentration of human genomic DNA may be determined by a couple of methods, but the most common approaches for biological samples require DNA material amplification with polymerase chain reaction (PCR) or branched DNA [2,3], which makes these techniques sophisticated, time-consuming, and highly dependent on human error [4,5]. Other methods for ultrasensitive detection of DNA material include spectrophotometric [4,6], fluorescence spectroscopy [7,8], or quartz-crystal microbalances [9]. Next, the detection of DNA denaturation could be conducted at diamond micro-cantilevers operating in dynamic mode in liquid environments. It was detected by physically by comparing the resonance frequency shift of the measuring diamond [10].

Recently, various electrochemical methods (potentiometric, voltammetric and impedimetric) find more and more utility for the hybridization and damage of DNA material [11–15]. None of these require DNA amplification, presenting an alternative for cost-efficient detection without, but electrochemical impedance spectroscopy stands out strongly, where the reported DNA hybridization detection limits ranges attomoles [16,17]. With some exceptions, the above given methods, however, suffer from low detection specificity [4].

The target single-stranded DNA (ssDNA) is anchored from the electrolyte to an electrode surface specifically-tailored by the complimentary oligonucleotide sequence, and leading to DNA hybridization. In electrochemical biosensing, the detection is based on measuring the anchoring-associated changes in charge transfer kinetics, and its comparison with the reference [18,19]. The electrode functionalization through the reduction of diazonium salt can lead to numerous processes, such as Suzuki cross-coupling [20] or Sonogashira reaction [21] etc. Different functionalization routes may be used for recognition of different macromolecules, such as proteins, enzymes or antibodies [18,22–24].

Boron doped diamond (BDD) electrodes are the foundations for creating new electrochemical biosensors platforms with very high sensitivity and selectivity for the selected analyte. These electrodes possess a wide electrochemical potential window and low background current what significantly increases not only the scope of analyzed electroactive compounds but also considerably influences the limit of detection [25]. Additionally, the BDD electrodes are characterized by high chemical resistance in aqueous and non-aqueous media, good resistance to fouling [26] and are regarded as biocompatible [27]. The desired features of the BDD electrode as biosensors are achieved through their surface functionalization by chemical methods [28]. Numerous studies reveal the possibility of BDD electrodes functionalization with tRNA, as well as single and double-stranded DNA chains or oligonucleotides [29,30]. Nebel et al. [31,32] proposed an electrochemical sensing platform based on BDD functionalized with specific ssDNA and allowing to detect DNA hybridization at the electrode surface. Yang et al. [33] obtained a strong binding preference to complementary versus non-complementary DNA sequences through photochemical functionalization.

Faradaic impedance spectroscopy is usually considered to be more sensitive to the insulation of the electrode surface upon the binding of bulky antibodies to the antigen-functionalized electrode surfaces, allowing to achieve low limits of detection, is the electrochemical impedance spectroscopy. The detection procedures of the impedance to biosensors are typically carried out in the presence of a redox couple, at its formal potential, to keep the system at its equilibrium state and maintaining stationary conditions throughout the experiment. However, performing the tests in potentiostatic conditions provides a major restriction since the differentiation between impedance response in the absence and presence of a studied analyte may be enhanced at certain polarization potentials. Recent DNA hybridization studies prove potentiodynamic conditions to be highly valuable for successful DNA assays. This situation is possible in particular when the differentiation factor results from varied kinetics of the adsorption/desorption process, such as nonspecific adsorption of the target DNA [34,35]. On the other hand, the application of electrochemical impedance spectroscopy (EIS) in non-linear and non-stationary conditions during potentiodynamic polarization is controversial.

Impedance measurements with multisine perturbation signal allow obtaining instantaneous impedance data for system characterized by dynamically changing conditions. This way, dynamic electrochemical impedance spectroscopy (DEIS) was successfully utilized to investigate non-stationary processes, such as various types of corrosion [36,37], erosion [38], but also fuel cells failure [39], polymer coatings [40] or adsorption processes [41]. More importantly, superimposing the multisine perturbation signal on linear sweep voltammetry (LSV) measurement offers significantly enhanced characteristics of the electrochemical processes occurring at the electrode interface. This includes electric parameters

3

derivatives as a function of time or polarization depth [42], allowing for a deep insight into nonspecific hybridized DNA adsorption. Taking the above into consideration, the authors have decided to utilize the DEIS technique to perform an attempt of DNA assay.

The target of this study is the beta-defensin 1 gene (DEFB1), which is present in the *Homo sapiens* genome and specific to the human DNA. The DEFB1 codes for an antimicrobial peptide implicated in the resistance of epithelial surfaces to microbial colonization. Thus, the above-mentioned gene can be used to distinguish between human and non-human DNA. Such a discrepancy would be useful in diagnostics [43] or forensic medicine when DNA samples of unknown origin are analyzed, where usually it is performed by antibody tests detecting human body fluid or PCR testing detecting human DNA. The following manuscript presents novel sensing approach of human DNA based on the evaluation of potentiodynamic DEIS (pDEIS) for saliva extracts of human origin with the reference to the analyte collected for selected mammals and bird species. To the best of the authors' knowledge, this is the first reported attempt to perform qualitative electrochemical analysis of complex macromolecular structures with multisine impedance technique.

2. Experimental

2.1 Materials and chemical reagents

All chemicals and solvents were analytical grade and were used without any further purification. Potassium ferrocyanide $K_4[Fe(CN)_6]$, hydrochloric acid, sodium nitrite and PBS buffer components were purchased from POCh (Poland), *N*-(3-dimethylaminopropyl)-*N'*-ethylcarbodiimide hydrochloride (EDC), *N*-hydroxysuccinimide (NHS) and 4-aminobenzoic acid were purchased from Sigma-Aldrich (USA). The commercially available amino-modified oligonucleotides used for tailored functionalization of BDD electrodes were purchased from Genomed (Poland). The sequence of oligonucleotide was amino- $(CH_2)_6$- 5'- CCC AGT TCC TGA AAT CCT GA-3', hereafter referred to as ssDNA probes.

The target DNA samples were obtained using the below-described procedure. Buccal swabs were collected from ten men and women and eleven animals: two guinea pigs, two geese, dog, two ducks, two cats, and two hens. DNA was isolated using the phenol-chloroform method. The swabs were incubated with 400 μl TE buffer pH 8.0, 20 μl proteinase K (20 mg ml^{-1}) and 13 μl 20% SDS overnight at 56°C. Then, the samples were extracted with phenol:chloroform:isoamyl alcohol mixture (25:24:1), and precipitated with absolute ethanol and 3 M sodium acetate. Precipitates were resuspended in Tris-HCl buffer (pH 8.5) and purified using microcolumns (Ultracel YM 100, Microcon) according to the manufacturer's protocol. The total DNA concentration was measured with a NanoDrop-1000 spectrophotometer (ThermoFisher Scientific, USA) following the manufacturer's protocol and its quantity

was normalized to 100 ng µl^{-1}. Finally, the solution containing extracted samples was heated at 95°C to unravel the DNA double-strand directly before the incubation at the electrode. It should be noted that samples contained DNA of an analyzed organism and microbes, in an unknown ratio, due to difficulties in measuring DNA of each species.

The BDD films were synthesized in a microwave plasma-assisted chemical vapor deposition system (SEKI Technotron AX5400S, Tokyo, Japan). The BBD electrodes were deposited on p-type silicon (100) plates with dimensions 10 x 10 mm, with 500 µm thickness and electric resistivity ranging 10 Ωcm. The Si substrates were cleaned in an ultrasonic bath for 2 min in acetone and 2-propanol, and next nucleated in water-based nanodiamond suspension (NanoAmando Aqueous Colloid, Japan) for 25 min. The optimized parameters set were 1% CH_4 of 300 sccm total gas flow and 2% of diborane (B_2H_6) which corresponds to 10000 ppm [B]/[C] ratio in the gas phase. The temperature of the heated stage was set to 700°C, microwave power to 1300 W, process pressure to 50 Torr. The time of the deposition was 6 h which results in approx. 3 µm thick diamond film [44].

Following the deposition process, a four-step pre-treatment of deposited BDD/Si electrodes was applied to obtain H-terminated surface and etch sp^2-carbon phase impurities. First, the removal of sp^2-carbon phase impurities by a hot "piranha" solution (H_2O_2:H_2SO_4 1:3, v-v) at 90°C, followed by hydrogen plasma treatment under following conditions, heated stage temperature was set to 500°C, microwave power to 1100 W, the pressure to 50 Torr and hydrogen flow to 300 sccm. The time of hydrogen plasma treatment was optimized to 10 min.

2.2 Modification, functionalization and incubation steps

Before their functionalization, the BDD electrodes were ultrasonically cleaned in methanol solution for 10 min, washed with distilled water and dried in air. In the first modification step, the BDD was electropolymerized by the reduction of diazonium salt of 4-aminobenzoic acid to generate carboxylic groups on the electrode surface. The modification procedure details are described elsewhere [18,45]. Following this step, the electrodes were washed with water and dried in air. The second step was the functionalization of the modified electrode with ssDNA probes. The prepared mixture was consisting of 0.10 M EDC and 0.05 M NHS in 0.10 M PBS, at pH = 7.4 [46]. A mixture composed of 50 µL oligonucleotide solution and 50 µL EDC/NHS was dropped on each modified BDD electrode. The ssDNA probe was covalently attached to the electrode surface through amide bonds during 1-hour functionalization.

Finally, the solution containing the studied analyte was incubated on the functionalized electrode surface at room temperature. A 100 µL of the solution containing 0.2 µM analyte in 0.1 M PBS was dropped at the electrode surface and left for 30 min. The DEFB1 gene concentration in the mixture used for incubation was 1 ng ml^{-1}. Both functionalization and incubation procedures were followed with the washing of the BDD electrode with 0.1 M PBS solution to remove unbounded DNA targets. The functionalization and incubation processes combined took 1.5 h, after which the BDD electrode was immediately used for electrochemical studies. The above-discussed procedures are schematically shown in **Fig. 1a**.

2.3 The electrochemical and physico-chemical methods

Electrochemical measurements were carried out in a three-electrode setup. Functionalized BDD served as the working electrode (electric contact provided at the back-side of the electrode). The electrode surface area exposed to electrochemical studies was 0.5 cm^2. Silver rod covered with silver chlorides (Ag|AgCl) served as the reference electrode and platinum mesh as the counter electrode. All electrochemical measurements were performed in 0.1 M PBS with 5.0 mM K$_4$[Fe(CN)$_6$], in the electrochemical cell with a volume of 8 mL. A more detailed discussion on the utilization of ferrocyanide ions is provided in the Supplementary Material. The electrolyte was purged with argon before each experiment.

The setup for electrochemical measurements consisted of Autolab 128N potentiostat (Metrohm, Netherlands) connected to two measurement cards (National Instruments, USA): PXI-4464 served for a generation of ac perturbation signal while PXI-6124 was used for acquisition of ac/dc response. Both these cards operated in PXIe-1073 chassis.

DEIS measurements were performed using a multifrequency perturbation signal composed of superimposed 29 elementary signals in frequency range was between 94 kHz and 7 Hz. The phase shift of each elementary signal was selected using optimization software written in LabView environment to minimize the resultant signal amplitude. The optimized multifrequency signal peak-to-peak amplitude did not exceed 15 mV. Such an approach allows to maintain the linearity regime. Detailed information about the construction of a multifrequency perturbation signal is presented elsewhere [47,48]. The sampling frequency was 204.8 kHz. The acquisition signal was sequenced with an analyzing window 1 s in length, then its sections were decomposed using Fourier Transform, which allowed to obtain instantaneous impedance spectra. Due to a large amount of the impedance spectra, the fitting procedure was performed using dedicated fitting software built in the LabView environment and based on the Nelder-Mead algorithm [49]. The impedance measurements were carried out simultaneously to the LSV study, realized

6

with the scan rate of 5 mV s^{-1}. The potentiodynamic polarization range was -1.0 to +1.0 V vs Ag|AgCl electrode. Selection of the scan rate derived from DEIS measurement restrictions. The limiting factor when choosing a scan rate is the length of the analytic window/single portion of the signal used for Fourier Transformation. When the applied scan rate is too high, the system non-stationarity degree is significant. Furthermore, the disproportion between scan rate and amplitude of ac multifrequency signal harms the quality of spectra.

The high-resolution X-ray photoelectron spectroscopy (XPS) studies were carried out in the binding energy range of *C1s* and *N1s* spectra, which allowed for the identification of functionalization efficiency. The analysis was carried out on the Escalab 250Xi spectroscope (ThermoFisher Scientific, USA), equipped in monochromatic AlKα source, with the spot diameter of 650 µm. Measurements were conducted using 15 eV pass energy and 0.05 eV energy step size. The charge compensation was controlled through low-energy electrons and low-energy Ar$^+$ ions emission through a flood gun. The spectral deconvolution was performed using Avantage v5.973 software (ThermoFisher Scientific, USA). Scanning electron microscope S-3400N (Hitachi, Japan) was used to image the surface of the BDD electrode. The microscope was operating in secondary electrons mode, with an accelerating voltage of 20 kV.

3. Results and discussion

Each step of BDD electrode modification and functionalization was monitored by EIS studies, carried out in open circuit potential conditions (see Supplementary Material, **Fig. S1**). These results confirm the significant increase in the charge transfer resistance R$_{CT}$, resulting from the formation and growth of the adsorbed functionalized layer, which is assisted by moderate changes of the quasi-capacitive parameter and electrode homogeneity. At the same time, the development of the functionalization layer is visible on SEM images and high-resolution XPS studies (**Fig. 1b-d**).

Fig. 1c shows the *C1s* spectra recorded for bare H-terminated BDD electrode before its modification. The spectrum is dominated by the presence of C(1) component at 284.3 eV, which was ascribed to *sp^3*-carbon rich hydrogen-terminated BDD substrate. The second, smaller component is typically attributed to non-hydrogenated carbon atoms in BDD or adsorbed polyhydride carbon species contaminating the electrode surface [50]. The successful modification of the BDD electrode surface with 4-aminobenzoic acid may be confirmed with the appearance of additional components on *C1s* spectra. The C(3) peak lies in the binding energy range characteristic to *sp^2*-carbon in benzene, while the positions of peaks C(4) and C(5) are commonly found in the amine (286.1 eV) and carboxyl (288.3 eV) functional

groups, respectively [51,52]. This observation was further confirmed by the appearance of *N1s* peak N(1) at 399.5 eV, which is characteristic of amine functional groups (**Fig. 1d**) [52]. Surface hydroxyl groups originating from 4-aminobenzoic acid overlap the previously defined C(2) peak at 285.1 eV.
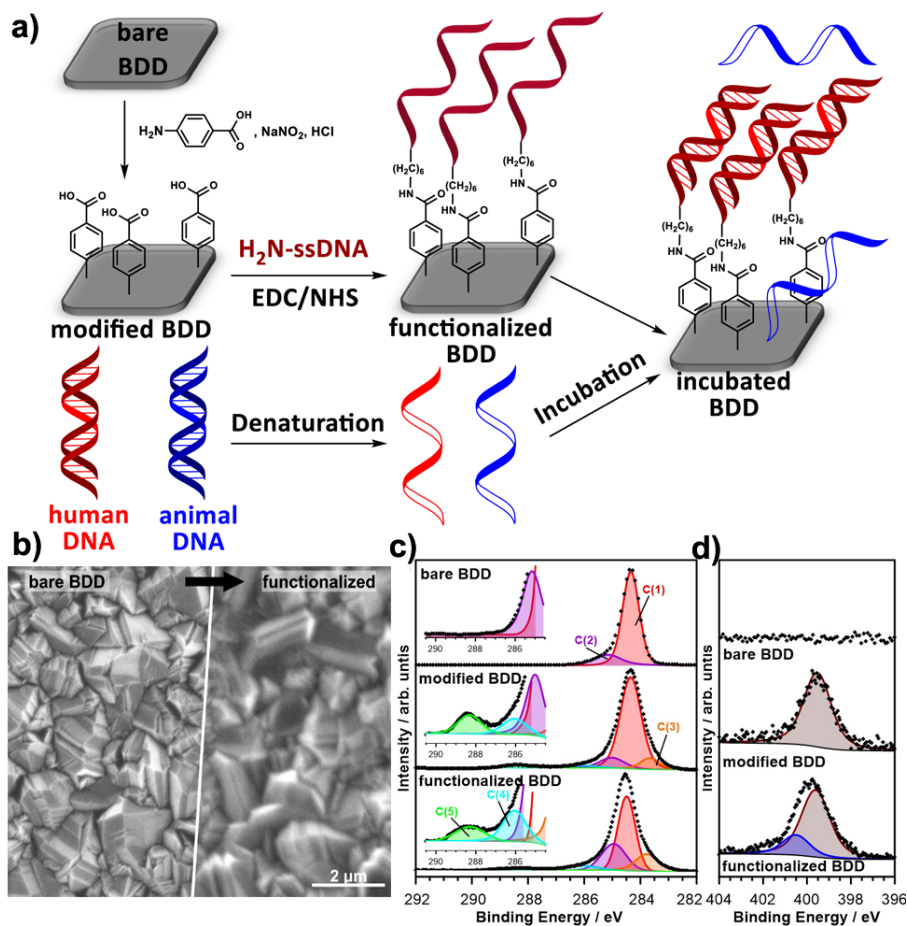

Fig. 1 – a) The scheme for BDD electrode modification with 4-aminobenzoic acid, its functionalization with DEB1-complimentary oligonucleotide sequence ssDNA and finally incubation with one of studied DNA material after its denaturation, b) SEM images illustrating topography of bare BDD electrode and BDD after modification and functionalization, c) high-resolution XPS spectra in the *C1s*, d) *N1s* binding energy range.

The functionalization of the previously modified BDD surface does not bring significant changes in surface carbon chemistry. Based on previous literature studies it should be assumed that the hydrocarbons within oligonucleotides will contribute the C(2) peak, carbon bound to nitrogen (C-N, N-C=N) will contribute C(4) peak, while amide carbon (N-C=O) and urea carbon (N-C(=O)-N) produce peaks shifted above 288 eV, contributing C(5) peak [53,54]. The functionalized layer naturally has a higher thickness, which, in consequence, produces a smaller signal from BDD substrate C(1). Moreover,

8

more complex nitrogen chemistry is represented by the appearance of N(2) peak on *N1s* spectra. The *N1s* spectra for all nucleobases except adenine consists of a strong signal peaking at region above 400 eV, which is attributed to amino N sites that connect with single bonds. On the other hand, the N(1) peak is enriched with the overlapping signal from imino species including N=C bond [53,54]. Full deconvolution data are summarized in Supplementary Material, **Table S1**.
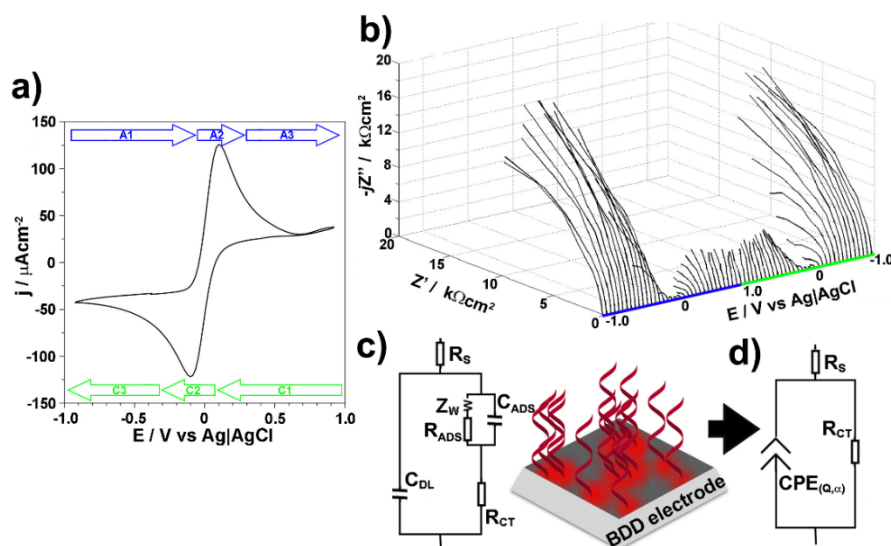

Fig. 2 – Exemplary pDEIS results for sample from Albert the pug: a) linear sweep voltammetry curve registered and b) corresponding potentiodynamic DEIS diagram in Nyquist projection with polarization potential at Z-axis, c) schematic representation of the electric equivalent circuit (EEC) commonly used to describe electrodes functionalized with organic macromolecules and the heterogeneity introduced by the adsorbed layer, d) simplified EEC used in this study.

As described within the experimental section, the multisine perturbation signal is superimposed with LSV scans during the potentiodynamic DEIS measurements. The exemplary voltammogram with the corresponding simultaneously-recorded DEIS spectra is shown in **Fig. 2a and 2b**, while all the LSV results are presented in the Supplementary Material, **Fig. S2**. The course of the polarization scan may be easily tracked based on the location of $Fe[(CN)_6]^{3-/4-}$ oxidation/reduction peak, where initiation of the redox process is directly linked with the decrease of measured impedance, visible in the form of a decrease in the capacitive loop dimensions. Three different stages of both the anodic and the cathodic scan should be distinguished, namely: preceding stage (A1/C1), ferrocyanide ions oxidation/reduction stage (A2/C2) and stage resultant from $Fe[(CN)_6]^{4-/3-}$ concentration drop at the interface (A3/C3) [55].

A two time-constants electric equivalent circuit EEC is often used in similar studies, as presented in **Fig. 2c**. The first time constant consists of charge transfer resistance (R_{CT}) and double layer capacitance

(C$_{DL}$), while the second one reflects the transition of the charge transfer through surface adsorbed layer (R$_{ADS}$, C$_{ADS}$). Finally, R$_S$ defines electrolyte resistance and Z$_W$ is Warburg element representing linear diffusion. When considering electrode heterogeneity effects in the double layer as well as sluggish charge transfer processes, authors often utilize constant phase element (CPE), which influences frequency dispersion [56]. The above-defined heterogeneity may be introduced by numerous features, including non-uniform site-specific charge transfer kinetics due to electrode polycrystallinity, 2D adsorption of macromolecules or contaminants, and resultant interspace regions but also electrode material geometry and porosity [57,58]. The impedance of the CPE is defined by two parameters, quasi-capacitance Q and exponent α, according to eq. (1):

$$Z_{CPE} = \frac{1}{Q(j\omega)^{\alpha}} \tag{1}$$

For an ideal capacitor α = 1, thus the CPE exponent is associated with the electrode heterogeneity, introduced by frequency dispersion of capacitance.

In the case of small site-specific variation of the charge transfer kinetics the resultant characteristic frequency where the influence of these heterogeneities is maximum is similar. Thus, the presence of a thin and discontinuous functionalization layer of anchored ssDNA probes or hybridized DNA in real conditions should be considered using a single-time constant EEC with frequency dispersion of capacitance. A similar conclusion may be drawn when analyzing the shape of the obtained impedance spectra. The final modification of the EEC presented in **Fig. 2d** is dictated by the frequency range used in the pDEIS experiment, having 7 Hz as the lowest elementary frequency in the multisine perturbation signal. The linear diffusion manifests itself at low frequencies (< 10 Hz) [52,59], thus its presence in the EEC is unjustified. To conclude, the EEC used within this study consists of a singular time constant, where R$_{CT}$ defines the charge transfer resistance through the electrode/electrolyte interface and CPE defines the frequency dispersion of the electric double layer and adsorbed layer capacitances.

Fitting of the pDEIS impedance spectra with EEC allows observing changes of the electric parameters during LSV polarization scan. The results for the anodic polarization are presented in **Fig. 3a-c** for charge transfer resistance and **Fig. 3d-i** for constant phase element parameters. The cathodic scan reveals no significant changes, therefore it was shown in Supplementary Material, **Fig. S3**.

The significant drop of the R$_{CT}$ during anodic polarization in A1 polarization range reflects charge accumulation at the electrode surface, leading to oxidation of the ferrocyanide electroactive species. This drop is visible for each analyzed sample, regardless of the DNA origin used during the incubation step, however, the initial R$_{CT}$ values may differ depending on various material features and functionalization efficiency. Next, the R$_{CT}$ minima are observed at the potential corresponding to the ferrocyanide oxidation

peak, where it reaches approx. 500 Ωcm^2. Again, this is observed regardless of the analyzed sample. A significant difference between the BDD electrode incubated in the presence of human DNA and any other DNA material is observed only in the last stage (referred to as A3 in **Fig. 2**). Here, the measured R_{CT} values for human DNA is nearly twice higher than in the case of any other investigated sample. This important feature should be explained by the altered behavior of electroactive species in the presence of a positively charged electrode surface covered with hybridized DNA material, as discussed further in the manuscript.
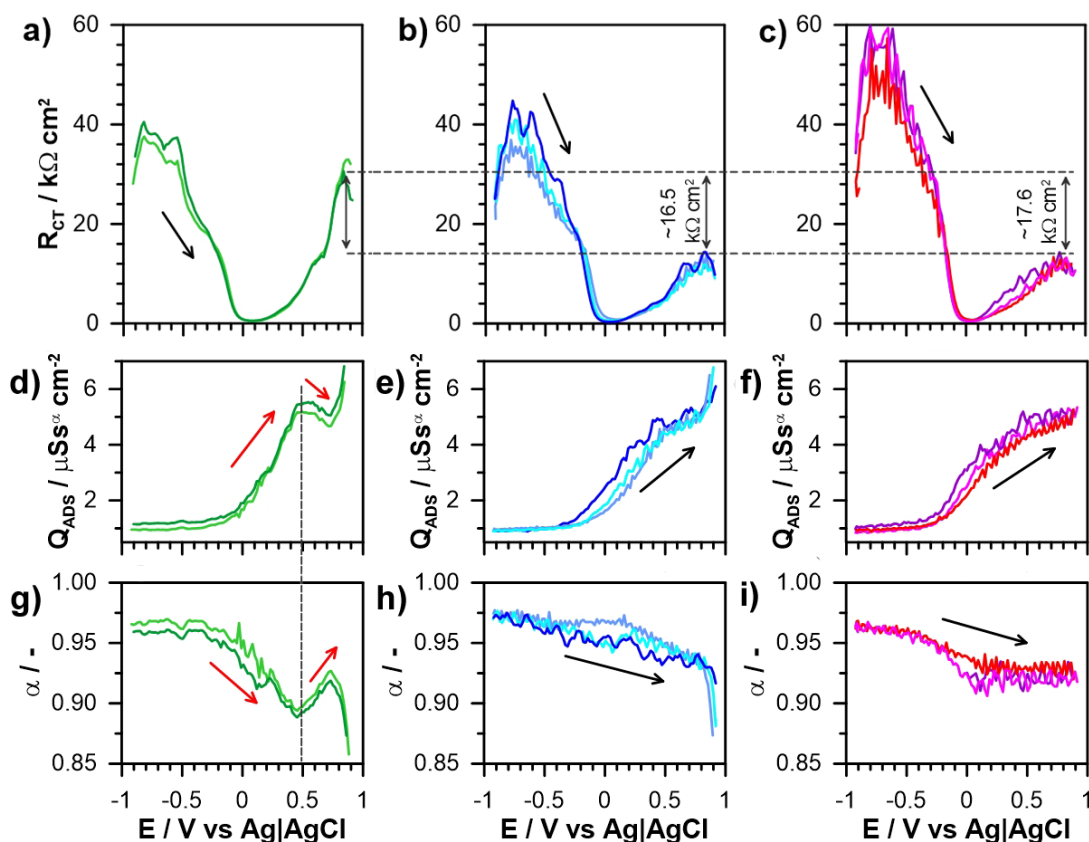
Fig. 3 – Instantaneous changes of R_{CT} parameter (a-c) and CPE parameters Q (d-f) and α (h-i), during anodic polarization scan, obtained with pDEIS for BDD electrodes incubated with various DNA material: a,d,g) human, b,e,h) household pets, c,f,i) domestic fowl. Scan rate 5 mV s^{-1}.

Comparing the course of quasi-capacitance changes during anodic polarization scan (**Fig. 3d-f**) one can observe the stability of this parameter in the stage preceding $Fe[(CN)_6]^{4-}$ ions oxidation (A1), a feature common for all the analyzed samples. Similarly, initiation of the oxidation process (stage A2) is accompanied by an increase in the quasi-capacitance parameter value. The quasi-capacitance parameter Q

11

is closely related to the C_{DL}, whereas the electric double layer is determined by the ions in the solution and at the electrode vicinity. Throughout A1 stage, the electrolyte composition is relatively constant, but after reaching A2 stage the anodic process intensifies, leading to a rapid decrease in $Fe[(CN)_6]^{4-}$ concentration and the increase in its oxidized form, $Fe[(CN)_6]^{3-}$, at the electrode/electrolyte interface. The effect of discussed changes is the observed increase in Q during stage A2 and partially A3 of the anodic polarization scan. However, the most important feature, diversifying the results obtained for the electrodes exposed to human DNA during the electrode incubation, is the appearance of a well-developed capacitive peak in the final polarization stage (A3), at 0.5 V vs Ag|AgCl. This feature is exclusive to incubated electrodes with human origin DNA material. Significantly, this peak also corresponds to the decrease in CPE exponent α value (**Fig. 3g-i**). Typically, measured changes in capacitance value are related with a combination of changes in electroactive surface area A, the relative permittivity of species present at the interface ε or the thickness of considered layer d, through a well-known relation:

$$C = \frac{\varepsilon_o \varepsilon d}{A} \tag{2}$$

where ε_0 is the vacuum permittivity. However, for analyses utilizing the CPE, electrode homogeneity and resultant capacitance dispersion have a significant influence on quasi-capacitance value, through eq. (1).

Higher levels of capacitance dispersion are always associated to phase transition phenomena that take place at the interface, even in the case of monocrystalline electrodes. Thus, the dispersion should not be exclusively attributed to the characteristics of the surface but rather the interfacial processes, primarily those taking place in the inner layer of the electric double layer [58]. The decrease of CPE exponent α seen throughout the anodic polarization process is a clear indication of the increase in capacitance dispersion and surface heterogeneity, observable on in the case of samples exposed to human DNA.

Both observable features differentiating human and non-human DNA, i.e. the charge transfer resistance as well as preceding homogeneity factor decrease, are introduced only when a positive electric field is built up at the electrode and only in the case of hybridized double stranded DNA (dsDNA). These features may be explained by the appearance of dsDNA nonspecific adsorption appearing when a positive electric field is built up at the electrode surface. Similar effects originating from nonspecific adsorption of target DNA were observed by other studies in their differential pulse voltammetry and impedance spectroscopy studies [34,60–63]. The alteration of the electron transfer at positively charged-up electrode interface should be explained with the presence of the coulombic repulsion between negatively-charged ferrocyanide ions in the buffer and negatively-charged DNA phosphate groups on the electrode surface, which partially hinders ferrocyanide diffusion to the surface [62]. This is schematically illustrated in **Fig. 4a**.
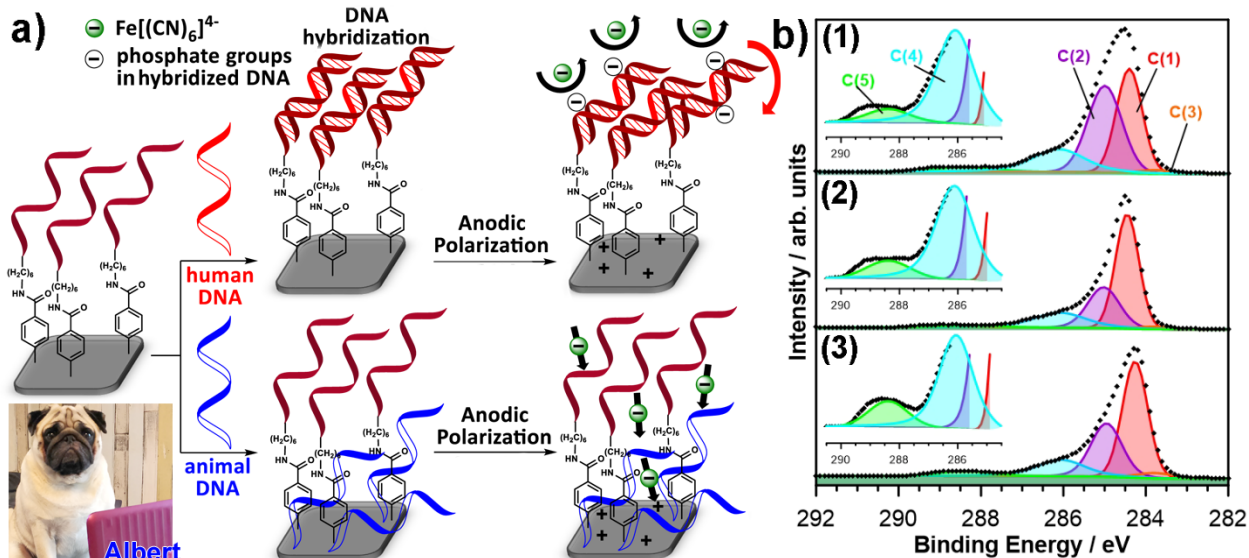
Fig. 4 – a) The schematic representation of the processes taking place at the functionalized BDD surface after its incubation with human or animal DNA material and when affected to anodic polarization in presence of ferrocyanide species, b) *C1s* XPS spectra recorded for the incubated sample exposed to (1) human DNA, (2) Albert the pug DNA, (3) geese DNA.

According to the previous examination, the tilt angle of DNA anchored on the BDD surface is around 33-36° [64,65]. It is plausible that the organization of the phosphate groups on the outside of hybridized dsDNA leads to their attraction towards a positively-charged electrode surface, and modifying the geometry of the anchored dsDNA. Such changes in hybridized DNA orientation in the electric field, assisted by potential-induced desorption of ssDNA from the surface are the reported reasons for the observed variations in the capacitance and fluorescence studies carried out by Meunier et al. [61]. The above-presented explanation is in good agreement with the observable changes in the adsorbed functionalization layer spatial homogeneity within this study. Naturally, this change precedes modification of the charge transfer resistance. The recorded frequency dispersion of capacitance offers a detailed pattern of altered behavior of the electrode with anchored DNA species, while the function of CPE exponent on the electrode potential allows us to reveal and monitor structuring effects, disturbing the nature of the Faradaic reactions.

The utilization of frequency dispersion to track subtle changes at the heterogeneous electrode interface finds confirmation in the earlier studies by the Bondarenka group [66–68], in their studies on potential-driven adsorption of bisulfates at the monocrystalline Pt surface. The above-mentioned studies revealed that the frequency dispersion effect is largely governed by 2D phase transitions in the adsorbed layers and in general by structural effects at the electrode/electrolyte interface. Similar observations were

13

made by our group on the polycrystalline electrode surfaces for carboxylic acid adsorption on the aluminium surface [52], but also in the case of the BDD electrodes [69].

Finally, **Fig. 4b** presents the exemplary representative *C1s* XPS spectra recorded for incubated BDD samples with DNA material of human origin, but also taken from pet (yes, it was Albert) and domestic fowl. The same deconvolution model was utilized as the one previously described. When comparing the surface chemistry of all three electrodes there are some qualitative changes visible. The major change applies to the intensity from the BDD substrate. For non-human samples, the share of C(1) component remains similar to the one observed in the case of the functionalized electrode, equal to 50.5% (change by 8%) and 47.9% (change by 3%) for Albert's and geese samples, respectively. However, the intensity of the C(1) signal after incubation with human DNA diminished to 35.4% (change by 24%). Similarly, a notable shift was observed in the case of C(2) component, which intensity for the BDD sample incubated with human ssDNA rise by 61% (its change for Albert and geese samples was 3 and 12%, respectively). To remind the reader, the primary source of the C(2) signal are hydrocarbon chains in the ssDNA probe. The observed shift of both these components is huge, suggesting an increase in the functionalization layer thickness or coverage due to anchoring human ssDNA to ssDNA probes during sample incubation, most likely leading to DNA hybridization. On the other hand, incubation of ssDNA of other origin leads to significantly smaller changes in the surface chemistry. Full deconvolution data are summarized in Supplementary Material, **Table S2**.

Moreover, DNA molecules are polyanions revealing negative charges at the phosphate backbone. Thus, the hybridization of the ssDNA probe molecule with its complementary ssDNA string involves charge transfer resulting in a modulation of the flat-band potential [70]. Nevertheless, the transfer of hybridization-induced signal is multi-factor dependent on i.e. the acid-base behavior, the density of the ssDNA layer, the length and orientation of DNA molecules, the length of linker molecules, the ionic strength of the buffer, as well as the electric field distribution at the electrode surface [71].

In the standard EIS conditions [72], the low frequencies attract migration of the polyvalent ions toward the electrode inducing DNA coil conformations and stabilizing weak attachment of nontargeted DNA molecules. Hence, the high frequencies suppress ions migration due to near charge relaxation times of the ions resulting in stretched DNA oligonucleotides conformations, which leads to improved detection sensitivity and selectivity. In our multisine approach, these both mechanisms are competing resulting in DNA conformations modulation, hence keeping oligonucleotides stretched by continual high-frequency component. This effect is attributed to the achieved high specificity of detection despite measurements in real samples. The reproducibility of the sensors was likewise satisfactory showing minor signal variations (below 5%) depending on the electrode set.

14

Similar to other studies on DNA detection, the charge transfer resistance was two times higher for dsDNA compared to ssDNA from other species (measured at +0.85 V), which might require further enhancement in order to prove its worth for forensic applications. Given the pDEIS was proved capable to detect subtle changes in dsDNA geometry at the electrode surface, it is possible that the disturbance of electrode homogeneity might be the route to further increase the detection limits. Such a situation would be achieved in the case of surface-modified nanoparticles self-assembling at the electrode surface in the electric field and due to biomolecular interactions [73,74].

4. Conclusions

We present a novel and efficient approach towards the detection of DNA hybridization under potentiodynamic conditions when a positive electric field is built up at the electrode surface. Within this study, we have utilized the discussed pDEIS approach to detect the presence of the DEFB1 gene, unique to human species, in collected saliva samples.

The detection process requires pre-treatment of the BDD electrode through tailored functionalization with oligonucleotide sequence, complementary to the DEFB1 gene sequence, which is anchored at the electrode surface. Next, a short-term incubation of the electrode in the presence of a target DNA sample allows achieving DNA hybridization when exposed to human DNA material. The DNA hybridization is not achieved in the case of non-complimentary ssDNA originated from any other species subjected to this test. The discussed differences obtained during electrode incubation are supported by the XPS analyses.

Next, given the hybridization is accomplished, its presence may be sensed through changes in electron transfer kinetics by ferrocyanide species at the positively-charged electrode surface. The observed increase in charge transfer resistance is preceded by subtle changes in frequency dispersion of capacitance as the positively-charged electrode surface affects the orientation of the hybridized dsDNA. We revealed that the impedimetric changes observed upon the formation of the bio-affinity complexes are potential-dependent and the optimal conditions for their measurement could be found. In this case, the highest shift in R_{CT} was observed at +0.85 V, preceded by CPE exponent α peak at approx. +0.50 V vs Ag|AgCl.

Our studies show that the DEFB1 gene can be used for a simple and rapid distinction between human and non-human material. Such an approach for specific DNA sequence detection can be an alternative for classic methods, usually involving PCR. The total length of the proposed DNA assay lasts for less than two hours. While PCR remains the gold standard of DNA testing, the above-described method, which does not require DNA amplification, provides new application perspectives. With the

15

capability to track the impedance changes as a function of applied polarization potential, our approach may surpass the DNA detection specificity offered by different electrochemical techniques, and in real conditions. Using other DNA sequences could provide possibilities like detection of pathogens, mutations, or polymorphisms, however additional research should be performed to fully evaluate these possibilities.

5. Acknowledgments

6. References

[1]   S. Kuga, J.-H. Yang, H. Takahashi, K. Hirama, T. Iwasaki, H. Kawarada, Detection of Mismatched DNA on Partially Negatively Charged Diamond Surfaces by Optical and Potentiometric Methods, J. Am. Chem. Soc. 130 (2008) 13251–13263. https://doi.org/10.1021/ja710167z.

[2]   H.-J. He, E.V. Stein, P. DeRose, K.D. Cole, Limitations of methods for measuring the concentration of human genomic DNA and oligonucleotide samples, BioTechniques. 64 (2018). https://doi.org/10.2144/btn-2017-0102.

[3]   X. Li, Y. Wu, L. Zhang, Y. Cao, Y. Li, J. Li, L. Zhu, G. Wu, Comparison of three common DNA concentration measurement methods, Analytical Biochemistry. 451 (2014) 18–24. https://doi.org/10.1016/j.ab.2014.01.016.

[4]   Y. Zhang, Z. Tang, J. Wang, H. Wu, A. Maham, Y. Lin, Hairpin DNA Switch for Ultrasensitive Spectrophotometric Detection of DNA Hybridization Based on Gold Nanoparticles and Enzyme Signal Amplification, Anal. Chem. 82 (2010) 6440–6446. https://doi.org/10.1021/ac1006238.

[5]   R.A. van Oorschot, K.N. Ballantyne, R.J. Mitchell, Forensic trace DNA: a review, Invest Genet. 1 (2010) 14. https://doi.org/10.1186/2041-2223-1-14.

[6]   W. Shen, H. Deng, Z. Gao, Gold Nanoparticle-Enabled Real-Time Ligation Chain Reaction for Ultrasensitive Detection of DNA, J. Am. Chem. Soc. 134 (2012) 14678–14681. https://doi.org/10.1021/ja306265n.

[7]   J. Zhou, Q. Wang, C. Zhang, Liposome–Quantum Dot Complexes Enable Multiplexed Detection of Attomolar DNAs without Target Amplification, J. Am. Chem. Soc. 135 (2013) 2056–2059. https://doi.org/10.1021/ja3110329.

[8]   A. Meunier, E. Triffaux, D. Bizzotto, C. Buess-Herman, T. Doneux, In Situ Fluorescence Microscopy Study of the Interfacial Inhomogeneity of DNA Mixed Self-Assembled Monolayers at Gold Electrodes, CHEMELECTROCHEM. 2 (2015) 434–442. https://doi.org/10.1002/celc.201402273.

[9]   L. Liu, C. Wu, S. Zhang, Ultrasensitive Detection of DNA and Ramos Cell Using In Situ Selective Crystallization Based Quartz Crystal Microbalance, Anal. Chem. 89 (2017) 4309–4313. https://doi.org/10.1021/acs.analchem.7b00411.

[10]   A. Bongrain, H. Uetsuka, L. Rousseau, L. Valbin, S. Saada, C. Gesset, E. Scorsone, G. Lissorgues, P. Bergonzo, Measurement of DNA denaturation on B-NCD coated diamond micro-cantilevers, Phys. Stat. Sol. (a). 207 (2010) 2078–2083. https://doi.org/10.1002/pssa.201000049.

[11] W. Białobrzeska, P. Niedziałkowski, N. Malinowska, Z. Cebula, T. Ossowski, Analysis of interactions between calf thymus DNA and 1,5-di(piperazin-1-yl)anthracene-9,10-dione using spectroscopic and electrochemical methods, Journal of Molecular Liquids. 289 (2019) 111080. https://doi.org/10.1016/j.molliq.2019.111080.

[12] A. Numnuam, K.Y. Chumbimuni-Torres, Y. Xiang, R. Bash, P. Thavarungkul, P. Kanatharana, E. Pretsch, J. Wang, E. Bakker, Potentiometric Detection of DNA Hybridization, J. Am. Chem. Soc. 130 (2008) 410–411. https://doi.org/10.1021/ja0775467.

[13] A. Benvidi, M.D. Tezerjani, S. Jahanbani, M. Mazloum Ardakani, S.M. Moshtaghioun, Comparison of impedimetric detection of DNA hybridization on the various biosensors based on modified glassy carbon electrodes with PANHS and nanomaterials of RGO and MWCNTs, Talanta. 147 (2016) 621–627. https://doi.org/10.1016/j.talanta.2015.10.043.

[14] M. Fojta, A. Daňhel, L. Havran, V. Vyskočil, Recent progress in electrochemical sensors and assays for DNA damage and repair, TrAC Trends in Analytical Chemistry. 79 (2016) 160–167. https://doi.org/10.1016/j.trac.2015.11.018.

[15] A. Kowalczyk, A.M. Nowicka, R. Jurczakowski, P. Niedzialkowski, T. Ossowski, Z. Stojek, New Anthraquinone Derivatives as Electrochemical Redox Indicators for the Visualization of the DNA Hybridization Process, Electroanalysis. 22 (2010) 49–59. https://doi.org/10.1002/elan.200900389.

[16] R.K. Shervedani, S. Pourbeyram, A modification free hybridization biosensor for detection of DNA sequence based on Zr(IV) ion glue mediated the adsorption on Au–MPA SAM electrode, Sensors and Actuators B: Chemical. 160 (2011) 145–153. https://doi.org/10.1016/j.snb.2011.07.025.

[17] A. Benvidi, N. Rajabzadeh, M. Mazloum-Ardakani, M.M. Heidari, Comparison of impedimetric detection of DNA hybridization on chemically and electrochemically functionalized multi-wall carbon nanotubes modified electrode, Sensors and Actuators B: Chemical. 207 (2015) 673–682. https://doi.org/10.1016/j.snb.2014.10.043.

[18] D. Nidzworski, K. Siuzdak, P. Niedziałkowski, R. Bogdanowicz, M. Sobaszek, J. Ryl, P. Weiher, M. Sawczak, E. Wnuk, W.A. Goddard, A. Jaramillo-Botero, T. Ossowski, A rapid-response ultrasensitive biosensor for influenza virus detection using antibody modified boron-doped diamond, Scientific Reports. 7 (2017) 15707. https://doi.org/10.1038/s41598-017-15806-7.

[19] K.-H. Lee, J.-O. Lee, M.-J. Sohn, B. Lee, S.-H. Choi, S.K. Kim, J.-B. Yoon, G.-H. Cho, One-chip electronic detection of DNA hybridization using precision impedance-based CMOS array sensor, Biosensors and Bioelectronics. 26 (2010) 1373–1379. https://doi.org/10.1016/j.bios.2010.07.055.

[20] Y.L. Zhong, K.P. Loh, A. Midya, Z.-K. Chen, Suzuki Coupling of Aryl Organics on Diamond, Chem. Mater. 20 (2008) 3137–3144. https://doi.org/10.1021/cm703686w.

[21] J. Raymakers, H. Krysova, A. Artemenko, J. Čermák, S.S. Nicley, P. Verstappen, S. Gielen, A. Kromka, K. Haenen, L. Kavan, W. Maes, B. Rezek, Functionalization of boron-doped diamond with a push–pull chromophore *via* Sonogashira and CuAAC chemistry, RSC Adv. 8 (2018) 33276–33290. https://doi.org/10.1039/C8RA07545J.

[22] Z. Salmi, A. Lamouri, P. Decorse, M. Jouini, A. Boussadi, J. Achard, A. Gicquel, S. Mahouche-Chergui, B. Carbonnier, M.M. Chehimi, Grafting polymer–protein bioconjugate to boron-doped diamond using aryl diazonium coupling agents, Diamond and Related Materials. 40 (2013) 60–68. https://doi.org/10.1016/j.diamond.2013.10.007.

[23] C. Cao, Y. Zhang, C. Jiang, M. Qi, G. Liu, Advances on Aryldiazonium Salt Chemistry Based Interfacial Fabrication for Sensing Applications, ACS Appl. Mater. Interfaces. 9 (2017) 5031–5049. https://doi.org/10.1021/acsami.6b16108.

[24] J.A. Ho, W.-L. Hsu, W.-C. Liao, J.-K. Chiu, M.-L. Chen, H.-C. Chang, C.-C. Li, Ultrasensitive electrochemical detection of biotin using electrically addressable site-oriented antibody immobilization approach via aminophenyl boronic acid, Biosensors and Bioelectronics. 26 (2010) 1021–1027. https://doi.org/10.1016/j.bios.2010.08.048.

[25] K. Muzyka, J. Sun, T.H. Fereja, Y. Lan, W. Zhang, G. Xu, Boron-doped diamond: current progress and challenges in view of electroanalytical applications, Anal. Methods. 11 (2019) 397–414. https://doi.org/10.1039/C8AY02197J.

[26] J.M. Freitas, T. da C. Oliveira, R.A.A. Munoz, E.M. Richter, Boron Doped Diamond Electrodes in Flow-Based Systems, Front. Chem. 7 (2019) 190. https://doi.org/10.3389/fchem.2019.00190.

[27] L. Tang, C. Tsai, W.W. Gerberich, L. Kruckeberg, D.R. Kania, Biocompatibility of chemical-vapour-deposited diamond, Biomaterials. 16 (1995) 483–488. https://doi.org/10.1016/0142-9612(95)98822-V.

[28] Y. Einaga, Diamond electrodes for electrochemical analysis, J Appl Electrochem. 40 (2010) 1807–1816. https://doi.org/10.1007/s10800-010-0112-z.

17

[29] C. Prado, G.-U. Flechsig, P. Gründler, J.S. Foord, F. Marken, R.G. Compton, Electrochemical analysis of nucleic acids at boron-doped diamond electrodes, Analyst. 127 (2002) 329–332. https://doi.org/10.1039/b111548k.

[30] T.A. Ivandini, B.V. Sarada, T.N. Rao, A. Fujishima, Electrochemical oxidation of underivatized-nucleic acids at highly boron-doped diamond electrodes, Analyst. 128 (2003) 924. https://doi.org/10.1039/b301483e.

[31] C.E. Nebel, N. Yang, H. Uetsuka, E. Osawa, N. Tokuda, O. Williams, Diamond nano-wires, a new approach towards next generation electrochemical gene sensor platforms, Diamond and Related Materials. 18 (2009) 910–917. https://doi.org/10.1016/j.diamond.2008.11.024.

[32] D. Shin, N. Tokuda, B. Rezek, C. Nebel, Periodically arranged benzene-linker molecules on boron-doped single-crystalline diamond films for DNA sensing, Electrochemistry Communications. 8 (2006) 844–850. https://doi.org/10.1016/j.elecom.2006.03.014.

[33] W. Yang, O. Auciello, J.E. Butler, W. Cai, J.A. Carlisle, J.E. Gerbi, D.M. Gruen, T. Knickerbocker, T.L. Lasseter, J.N. Russell, L.M. Smith, R.J. Hamers, DNA-modified nanocrystalline diamond thin-films as stable, biologically active substrates, Nature Mater. 1 (2002) 253–257. https://doi.org/10.1038/nmat779.

[34] Ľ. Švorc, D. Jambrec, M. Vojs, S. Barwe, J. Clausmeyer, P. Michniak, M. Marton, W. Schuhmann, Doping Level of Boron-Doped Diamond Electrodes Controls the Grafting Density of Functional Groups for DNA Assays, ACS Appl. Mater. Interfaces. 7 (2015) 18949–18956. https://doi.org/10.1021/acsami.5b06394.

[35] H. Gu, X. di Su, K.P. Loh, Electrochemical Impedance Sensing of DNA Hybridization on Conducting Polymer Film-Modified Diamond, J. Phys. Chem. B. 109 (2005) 13611–13618. https://doi.org/10.1021/jp050625p.

[36] K. Darowicki, S. Krakowiak, P. Slepski, The time dependence of pit creation impedance spectra, Electrochemistry Communications. 6 (2004) 860–866. https://doi.org/10.1016/j.elecom.2004.06.010.

[37] H. Gerengi, K. Darowicki, P. Slepski, G. Bereket, J. Ryl, Investigation effect of benzotriazole on the corrosion of brass-MM55 alloy in artificial seawater by dynamic EIS, Journal of Solid State Electrochemistry. 14 (2010) 897–902. https://doi.org/10.1007/s10008-009-0923-1.

[38] J. Ryl, K. Darowicki, P. Slepski, Evaluation of cavitation erosion–corrosion degradation of mild steel by means of dynamic impedance spectroscopy in galvanostatic mode, Corrosion Science. 53 (2011) 1873–1879. https://doi.org/10.1016/j.corsci.2011.02.004.

[39] K. Darowicki, E. Janicka, M. Mielniczek, A. Zielinski, L. Gawel, J. Mitzel, J. Hunger, The influence of dynamic load changes on temporary impedance in hydrogen fuel cells, selection and validation of the electrical equivalent circuit, Applied Energy. 251 (2019) 113396. https://doi.org/10.1016/j.apenergy.2019.113396.

[40] K. Darowicki, M. Szocinski, Evaluating the performance of organic coatings under mechanical stress using electrochemical impedance spectroscopy, Journal of Solid State Electrochemistry. 8 (2004) 346–351. https://doi.org/10.1007/s10008-003-0451-3.

[41] J. Ryl, J. Wysocka, M. Cieslik, H. Gerengi, T. Ossowski, S. Krakowiak, P. Niedzialkowski, Understanding the origin of high corrosion inhibition efficiency of bee products towards aluminium alloys in alkaline environments, Electrochimica Acta. 304 (2019) 263–274. https://doi.org/10.1016/j.electacta.2019.03.012.

[42] J. Ryl, L. Burczyk, R. Bogdanowicz, M. Sobaszek, K. Darowicki, Study on surface termination of boron-doped diamond electrodes under anodic polarization in H 2 SO 4 by means of dynamic impedance technique, Carbon. 96 (2016) 1093–1105. https://doi.org/10.1016/j.carbon.2015.10.064.

[43] E. Andresen, G. Günther, J. Bullwinkel, C. Lange, H. Heine, Increased Expression of Beta-Defensin 1 (DEFB1) in Chronic Obstructive Pulmonary Disease, PLoS ONE. 6 (2011) e21898. https://doi.org/10.1371/journal.pone.0021898.

[44] M. Ficek, R. Bogdanowicz, J. Ryl, Nanocrystalline CVD Diamond Coatings on Fused Silica Optical Fibres: Optical Properties Study, Acta Phys. Pol. A. 127 (2015) 868–873. https://doi.org/10.12693/APhysPolA.127.868.

[45] K. Siuzdak, P. Niedziałkowski, M. Sobaszek, T. Łęga, M. Sawczak, E. Czaczyk, K. Dziąbowska, T. Ossowski, D. Nidzworski, R. Bogdanowicz, Biomolecular influenza virus detection based on the electrochemical impedance spectroscopy using the nanocrystalline boron-doped diamond electrodes with covalently bound antibodies, Sensors and Actuators B: Chemical. 280 (2019) 263–271. https://doi.org/10.1016/j.snb.2018.10.005.

[46] K. Malecka, L. Michalczuk, H. Radecka, J. Radecki, Ion-Channel Genosensor for the Detection of Specific DNA Sequences Derived from Plum Pox Virus in Plant Extracts, Sensors. 14 (2014) 18611–18624. https://doi.org/10.3390/s141018611.

[47] P. Slepski, K. Darowicki, E. Janicka, G. Lentka, A complete impedance analysis of electrochemical cells used as energy sources, Journal of Solid State Electrochemistry. 16 (2012) 3539–3549. https://doi.org/10.1007/s10008-012-1825-1.

[48] P. Slepski, K. Darowicki, M. Kopczyk, A. Sierczynska, K. Andrearczyk, Electrochemical impedance studies of AB5-type hydrogen storage alloy, Journal of Power Sources. 195 (2010) 2457–2462. https://doi.org/10.1016/j.jpowsour.2009.11.089.

[49] F. Gao, L. Han, Implementing the Nelder-Mead simplex algorithm with adaptive parameters, Computational Optimization and Applications. 51 (2012) 259–277. https://doi.org/10.1007/s10589-010-9329-3.

[50] J. Ryl, M. Cieslik, A. Zielinski, M. Ficek, B. Dec, K. Darowicki, R. Bogdanowicz, High-Temperature Oxidation of Heavy Boron-Doped Diamond Electrodes: Microstructural and Electrochemical Performance Modification, Materials. 13 (2020) 964. https://doi.org/10.3390/ma13040964.

[51] J.S. Stevens, A. Gainar, C. Jaye, D.A. Fischer, S.L.M. Schroeder, NEXAFS and XPS of p-Aminobenzoic Acid Polymorphs: The Influence of Local Environment, J. Phys.: Conf. Ser. 712 (2016) 012133. https://doi.org/10.1088/1742-6596/712/1/012133.

[52] J. Wysocka, M. Cieslik, S. Krakowiak, J. Ryl, Carboxylic acids as efficient corrosion inhibitors of aluminium alloys in alkaline media, Electrochimica Acta. 289 (2018) 175–192. https://doi.org/10.1016/j.electacta.2018.08.070.

[53] S. Ptasińska, A. Stypczyńska, T. Nixon, N.J. Mason, D.V. Klyachko, L. Sanche, X-ray induced damage in DNA monitored by X-ray photoelectron spectroscopy, The Journal of Chemical Physics. 129 (2008) 065102. https://doi.org/10.1063/1.2961027.

[54] M.O. Silva-Moraes, Y. Garcia-Basabe, R.F.B. de Souza, A.J. Mota, R.R. Passos, D. Galante, H.D. Fonseca Filho, Y. Romaguera-Barcelay, M.L.M. Rocco, W.R. Brito, Geometry-dependent DNA-TiO2 immobilization mechanism: A spectroscopic approach, Spectrochimica Acta Part A: Molecular and Biomolecular Spectroscopy. 199 (2018) 349–355. https://doi.org/10.1016/j.saa.2018.03.081.

[55] A.J. Bard, L.R. Faulkner, Electrochemical methods: fundamentals and applications, 2nd ed, Wiley, New York, 2001.

[56] G.J. Brug, A.L.G. van den Eeden, M. Sluyters-Rehbach, J.H. Sluyters, The analysis of electrode impedances complicated by the presence of a constant phase element, Journal of Electroanalytical Chemistry and Interfacial Electrochemistry. 176 (1984) 275–295. https://doi.org/10.1016/S0022-0728(84)80324-1.

[57] S. Dhillon, R. Kant, Theory for electrochemical impedance spectroscopy of heterogeneous electrode with distributed capacitance and charge transfer resistance, J Chem Sci. 129 (2017) 1277–1292. https://doi.org/10.1007/s12039-017-1335-x.

[58] R.S. Neves, E. De Robertis, A.J. Motheo, Capacitance dispersion in electrochemical impedance spectroscopy measurements of iodide adsorption on Au(111), Applied Surface Science. 253 (2006) 1379–1386. https://doi.org/10.1016/j.apsusc.2006.02.010.

[59] T.Q. Nguyen, C. Breitkopf, Determination of Diffusion Coefficients Using Impedance Spectroscopy Data, J. Electrochem. Soc. 165 (2018) E826–E831. https://doi.org/10.1149/2.1151814jes.

[60] M.D.N. Ngavouka, P. Capaldo, E. Ambrosetti, G. Scoles, L. Casalis, P. Parisse, Mismatch detection in DNA monolayers by atomic force microscopy and electrochemical impedance spectroscopy, Beilstein J. Nanotechnol. 7 (2016) 220–227. https://doi.org/10.3762/bjnano.7.20.

[61] A. Meunier, E. Triffaux, D. Bizzotto, C. Buess-Herman, T. Doneux, In Situ Fluorescence Microscopy Study of the Interfacial Inhomogeneity of DNA Mixed Self-Assembled Monolayers at Gold Electrodes, CHEMELECTROCHEM. 2 (2015) 434–442. https://doi.org/10.1002/celc.201402273.

[62] A.A.I. Sina, L.G. Carrascosa, Z. Liang, Y.S. Grewal, A. Wardiana, M.J.A. Shiddiky, R.A. Gardiner, H. Samaratunga, M.K. Gandhi, R.J. Scott, D. Korbie, M. Trau, Epigenetically reprogrammed methylation landscape drives the DNA self-assembly and serves as a universal cancer biomarker, Nat Commun. 9 (2018) 4915. https://doi.org/10.1038/s41467-018-07214-w.

[63] J. Tymoczko, W. Schuhmann, M. Gebala, Electrical Potential-Assisted DNA Hybridization. How to Mitigate Electrostatics for Surface DNA Hybridization, ACS Appl. Mater. Interfaces. 6 (2014) 21851–21858. https://doi.org/10.1021/am5027902.

[64] C.E. Nebel, D. Shin, B. Rezek, N. Tokuda, H. Uetsuka, H. Watanabe, Diamond and biology, J. R. Soc. Interface. 4 (2007) 439–461. https://doi.org/10.1098/rsif.2006.0196.

[65] B. Rezek, D. Shin, T. Nakamura, C.E. Nebel, Geometric Properties of Covalently Bonded DNA on Single-Crystalline Diamond, J. Am. Chem. Soc. 128 (2006) 3884–3885. https://doi.org/10.1021/ja058181y.

[66] A.S. Bondarenko, I.E.L. Stephens, H.A. Hansen, F.J. Pérez-Alonso, V. Tripkovic, T.P. Johansson, J. Rossmeisl, J.K. Nørskov, I. Chorkendorff, The Pt(111)/Electrolyte Interface under Oxygen Reduction

Reaction Conditions: An Electrochemical Impedance Spectroscopy Study, Langmuir. 27 (2011) 2058–2066. https://doi.org/10.1021/la1042475.

[67] J. Tymoczko, V. Colic, A.S. Bandarenka, W. Schuhmann, Detection of 2D phase transitions at the electrode/electrolyte interface using electrochemical impedance spectroscopy, Surface Science. 631 (2015) 81–87. https://doi.org/10.1016/j.susc.2014.04.014.

[68] J. Tymoczko, W. Schuhmann, A.S. Bandarenka, The constant phase element reveals 2D phase transitions in adsorbate layers at the electrode/electrolyte interfaces, Electrochemistry Communications. 27 (2013) 42–45. https://doi.org/10.1016/j.elecom.2012.11.001.

[69] J. Ryl, L. Burczyk, A. Zielinski, M. Ficek, A. Franczak, R. Bogdanowicz, K. Darowicki, Heterogeneous oxidation of highly boron-doped diamond electrodes and its influence on the surface distribution of electrochemical activity, Electrochimica Acta. 297 (2019) 1018–1027. https://doi.org/10.1016/j.electacta.2018.12.050.

[70] A.A. Poghossian, Determination of the pHpzc of insulators surface from capacitance–voltage characteristics of MIS and EIS structures, Sensors and Actuators B: Chemical. 44 (1997) 551–553. https://doi.org/10.1016/S0925-4005(97)00156-1.

[71] M.H. Abouzar, A. Poghossian, A.G. Cherstvy, A.M. Pedraza, S. Ingebrandt, M.J. Schöning, Label-free electrical detection of DNA by means of field-effect nanoplate capacitors: Experiments and modeling, Phys. Status Solidi A. 209 (2012) 925–934. https://doi.org/10.1002/pssa.201100710.

[72] S. Basuray, S. Senapati, A. Aijian, A.R. Mahon, H.-C. Chang, Shear and AC Field Enhanced Carbon Nanotube Impedance Assay for Rapid, Sensitive, and Mismatch-Discriminating DNA Hybridization, ACS Nano. 3 (2009) 1823–1830. https://doi.org/10.1021/nn9004632.

[73] H.-I. Peng, B.L. Miller, Recent advancements in optical DNA biosensors: Exploiting the plasmonic effects of metal nanoparticles, Analyst. 136 (2011) 436–447. https://doi.org/10.1039/C0AN00636J.

[74] R.S.J. Alkasir, M. Ganesana, Y.-H. Won, L. Stanciu, S. Andreescu, Enzyme functionalized nanoparticles for electrochemical biosensors: A comparative study with applications for the detection of bisphenol A, Biosensors and Bioelectronics. 26 (2010) 43–49. https://doi.org/10.1016/j.bios.2010.05.001.

Supplementary Material

for

Multisine impedimetric probing of biocatalytic reactions for label-free detection of DEFB1 gene: How to verify that your dog is not human?

Pawel Niedzialkowski[1], Pawel Slepski[2], Joanna Wysocka[2], Joanna Chamier-Cieminska[3], Lukasz Burczyk[2], Michal Sobaszek[2], Anna Wcislo[1], Tadeusz Ossowski[1], Robert Bogdanowicz[2], Jacek Ryl[2,*]

[1] University of Gdansk, Wita Stwosza 63, 80-952 Gdansk, Poland
[2] Gdansk University of Technology, Narutowicza 11/12, 80-233 Gdansk, Poland
[3] Medical University of Gdansk, Debowa 23, 80-204 Gdansk, Poland
*Corresponding author: jacek.ryl@pg.edu.pl

1. The influence of the modification and functionalization steps on BDD surface chemistry

A derivative of Randles electric equivalent circuit (EEC) was chosen, for the reasons discussed later in the manuscript. The capacitance was replaced with a constant phase element (CPE) to simulate heterogeneities at the electrode surface. It is visible that each modification step contributes to the increase in electrode's charge transfer resistance (Fig. S1), with the final functionalization step modifying the R_{CT} value vs bare BDD electrode over 7 times, measured at open circuit potential conditions. This is a characteristic feature to any electrode functionalization process, deriving from formation of ssDNA adsorption layer limiting the electron transfer at the electrode/electrolyte interface. At the same time, both modification and functionalization steps have a moderate influence on the quasi-capacitance parameter Q, slightly increasing electrode homogeneity, represented by the CPE exponent α. Similar behavior is often observed as a result of the electrode functionalization step [1].
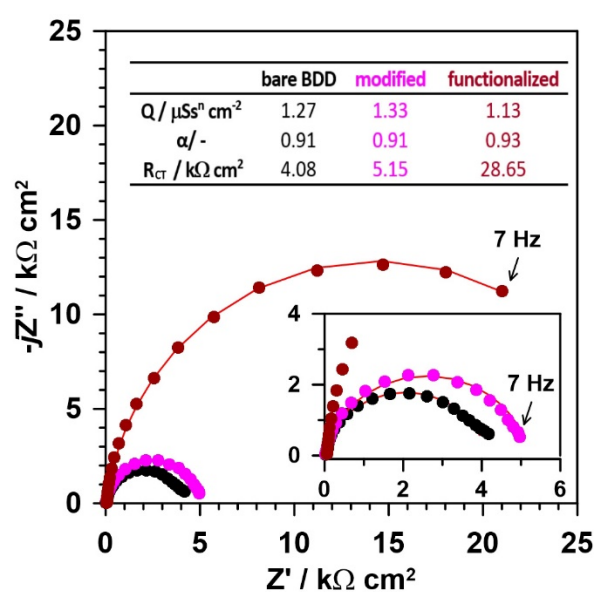

	bare BDD	modified	functionalized
Q / $\mu Ss^n\,cm^{-2}$	1.27	1.33	1.13
α / -	0.91	0.91	0.93
R_{CT} / $k\Omega\,cm^2$	4.08	5.15	28.65

Fig. S1 – EIS spectra projected in the form of Nyquist plot, illustrating impedance parameters changes as a result of BDD electrode modification and functionalization. Points represents experimental data and solid line fitting quality.

2. The linear sweep voltammetry scan of each studied electrode

The LSV stands as the most popular and commonly used electrochemical tool to be used in electroanalysis. The obtained LSV results for selected and representative samples containing human-DNA (Fig. S2a) were compared with non-human-DNA of pets (Albert the pug, cats and guinea pig) and domestic fowl (gooses, hens, ducks) shown on Fig. S2b and S2c, respectively.
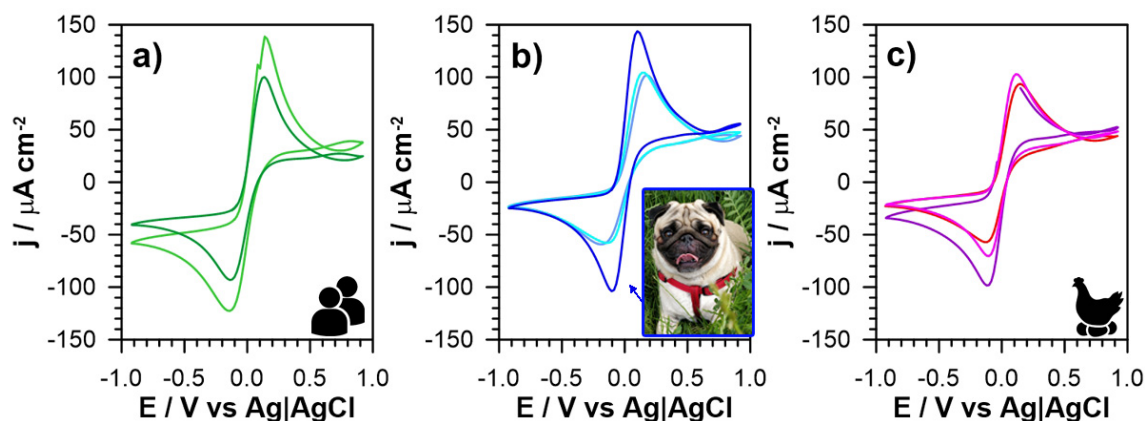

Fig. S2 – LSV scans for the BDD electrodes after their functionalization and incubation in presence of various DNA material: a) human, b) household pets, c) domestic fowl. Scan rate 5 mV/s.

Comparison of LSV results registered in electrolyte containing $[Fe(CN)_6]^{4-}$ ions does not bring any decisive results. Two well-defined peaks are observed after incubation in DNA samples in all the investigated cases. The highest peaks currents are observed in voltammograms obtained after incubation in solution containing human DNA (Fig. S2a), with peak-to-peak separation ΔE_p of 225 mV. A slight decrease of peak currents are observed after incubation in solution containing some of the household pets and domestic fowl with peak-to peak-separation ΔE_p ranging between 190 and 205 mV.

The LSV scans recorded for Albert the pug sample were characterized with high values of anodic and cathodic peak currents, similar to human specimens. This result suggests smaller restrictions in the charge transfer process for human and pug specimens, yet (to Albert's dissatisfaction) we believe this effect to be random and connected with variable kinetics of functionalized electrode charge transfer kinetics. This parameter depends not only on crystallographic structure of BDD electrode, crystal size, texture, but also local and completely unpredictable differences in thickness of organic macromolecular functionalization layer on top of BDD electrode surface.

3. The instantaneous electric parameters changes during cathodic polarization scan

Figure S3 reveals the change in recorded electric parameters based on pDEIS studies during cathodic polarization scan. These parameters develop in similar fashion as in the case of anodic polarization scan, excluding lack of the distinctive peak for Q_{ADS} and α parameters. At the same time, the R_{CT} parameter of the sample exposed to human DNA material remains significantly higher at deep anodic polarization.
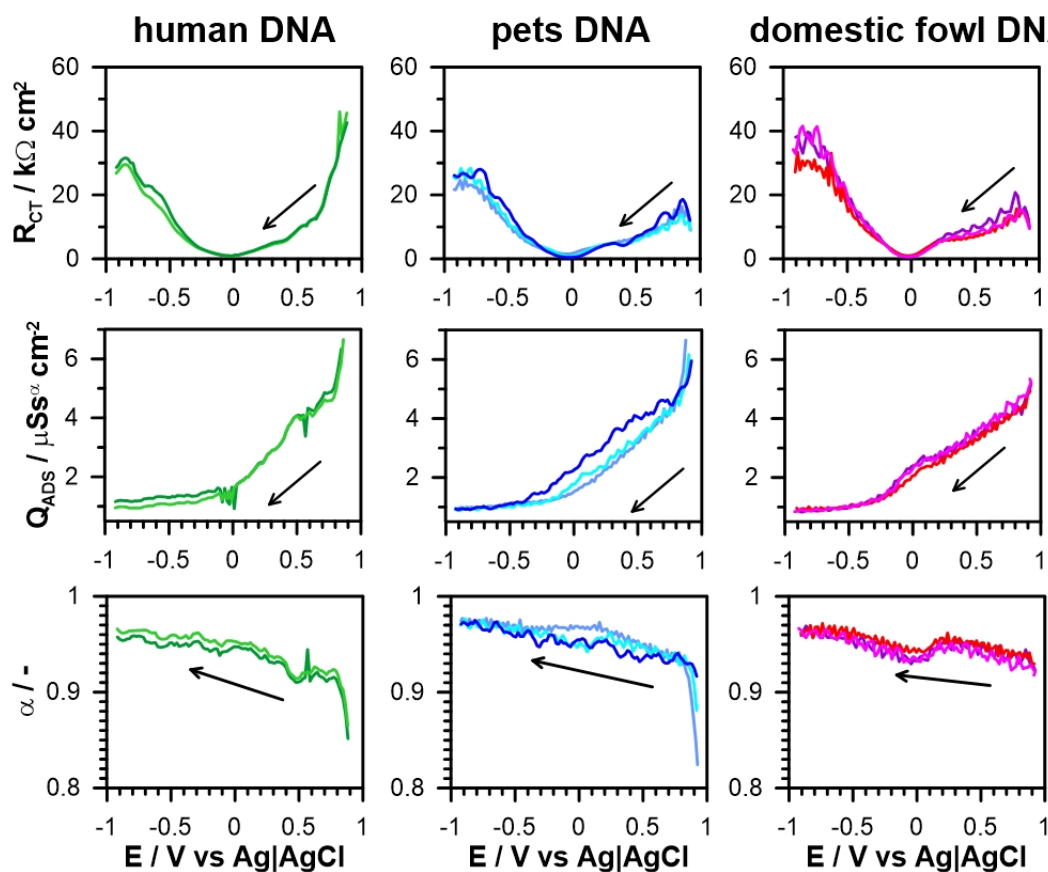

Fig. S3 – Instantaneous changes of R_{CT}, Q_{ADS} and α parameters during cathodic polarization scan, obtained with pDEIS for BDD electrodes incubated with various DNA material: a) human, b) household pets, c) domestic fowl. Scan rate 5 mV s⁻¹.

4. The effective capacitance after heterogeneity normalization

The influence of the capacitance dispersion factor on the adsorbed functionalization layer capacitance may be normalized using surface time-constant distribution model, where rise of capacitance dispersion results from variation of properties along the surface [2]. In this model, the effective capacitance C_{EFF} is given with eq. (S1).

$$C_{EFF} = Q^{1/\alpha} \left(\frac{R_S R_{CT}}{R_S + R_{CT}} \right)^{(1-\alpha)/\alpha} \tag{S1}$$

The changes of the C_{EFF} as a function of anodic polarization potential for each studies electrode may be tracked on Fig. S4.
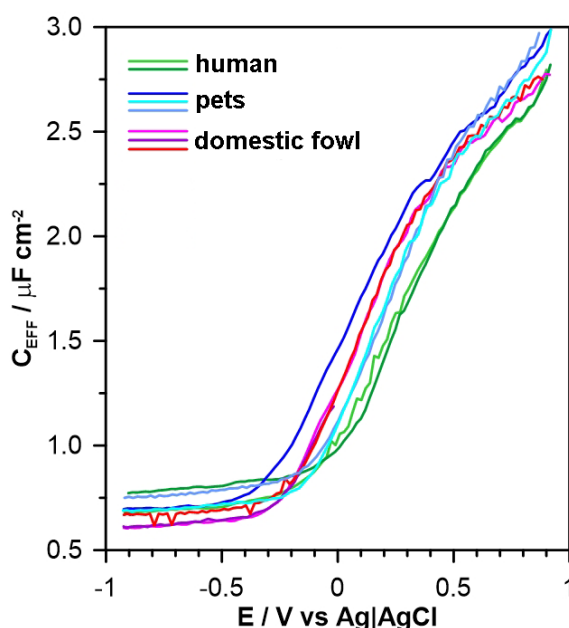

Fig. S4 – Effective capacitance C_{EFF} changes as a function of anodic polarization potential for all the studied electrodes.

Importantly, the quasi-capacitive peak, unique to samples with human DNA, is gone, thus confirming that the observed behavior was strictly connected to modulation of the electric heterogeneity at the interface due to frequency dispersion of capacitance. Furthermore, it should be noted that the molecular interactions are amplified at the surface by the two-dimensional nature of the immobilized functionalization layer, which focuses the nucleic acid charge and concentration to levels not encountered in solution, and which impacts the hybridization behavior in unique ways [3].

5. Detailed XPS deconvolution data

Tables S1 and S2 presents details of the deconvolution model used for the high-resolution XPS spectra analysis.

Table S1 – Chemical composition (in at.%) of various carbon and nitrogen chemical states on the surface of BDD electrode before and after consecutive modification and functionalization steps, based on high-resolution XPS analysis. Here, ↓↓ suggests the interpretation of the model is the same as in previously presented data.

	C1s					*N1s*	
	C(1) 284.3	C(2) 285.1	C(3) 283.6	C(4) 286.1	C(5) 288.3	N(1) 399.5	N(2) 400.6
Bare BDD	$CC_{HT\text{-}BDD}$ 88.6	$CC_{OT\text{-}BDD}$ 11.4	-- --	-- --	-- --	-- --	-- --
Modified BDD	↓↓ 69.8	also C-OH$_{mod}$ 11.0	CC-sp^2 9.5	C-NH$_2$ 3.8	COOH 4.5	NH$_2$-C 1.5	-- --
Functionalized BDD	↓↓ 46.6	also C-C 24.0	↓↓ 13.8	also C-N, NC=N 9.2	also NC=O 3.5	also N=C 0.6	also >NH 2.2

Table S2 – Chemical composition (in at.%) of various carbon chemical states on the surface of functionalized BDD electrode after its incubation with DNA of various origin, based on high-resolution XPS analysis.

Incubated BDD	*C1s*					*N1s*	
	C(1) 284.3	C(2) 285.1	C(3) 283.6	C(4) 286.1	C(5) 288.3	N(1) 399.5	N(2) 400.6
	$CC_{HT\text{-}BDD}$	C-C, C-OH	CC-sp^2	C-O, C-N, NC=N	COOH, NC=O	C-N, C=N	>NH
Human DNA	35.4	38.8	2.0	18.2	3.7	0.7	1.3
Albert the pug DNA	50.5	24.9	2.2	17.1	3.1	1.2	1.0
Geese DNA	47.9	27.1	3.5	14.5	4.1	1.7	1.1

6. Other remarks

6.1 Regarding utilization of the BDD electrodes

It should be noted, that apart from numerous reported desirable properties of the BDD substrates to be used in electroanalysis polycrystalline BDD is also known for its heterogeneity where the local distribution of electric properties depends on B-dopant density, crystallographic orientation, surface pretreatment methods, degree of sp^2-carbon contamination and others [4,5]. All of the above factors create difficulty to obtain reproducible conditions. In particular, the value of charge transfer resistance may be significantly different in-between samples. The following restriction does not apply to the proposed pDEIS approach since the object of evaluation is the relative change of electric parameters during the polarization scan. Thus, BDD was found to be the right material to demonstrate the advantages of the proposed approach.

6.2 Regarding utilization of ferrocyanides

The ferrocyanides are chemically inert compounds for biomolecules such as proteins or DNA. Their electrochemistry is well described in the literature, which makes them a good choice for various electrochemical sensing applications [6,7]. Furthermore, these negatively charged species are very sensitivity to monolayer adsorption on the electrode surface [8]. The $[Fe(CN)_6]^{3-/4-}$ redox couple are characterized by the inner sphere electron transfer (ISET) mechanism, which requires for a covalent bond to be formed on the electrode surface during the charge transfer process. Therefore, ISET electroactive species are known to be highly dependent on the electrode conditions or applied pre-treatment procedures, a feature which is welcome for the comparison purposes [9]. The use of negatively-charged ferrocyanide ions cause the coulombic repulsion with negatively-charged DNA phosphate groups present at the electrode surface what partially hinders ferrocyanide diffusion [10].

7. References:

[1] R.K. Shervedani, S.A. Mozaffari, Impedimetric sensing of uranyl ion based on phosphate functionalized cysteamine self-assembled monolayers, Analytica Chimica Acta. 562 (2006) 223–228. https://doi.org/10.1016/j.aca.2006.01.046.

[2] B. Hirschorn, M.E. Orazem, B. Tribollet, V. Vivier, I. Frateur, M. Musiani, Determination of effective capacitance and film thickness from constant-phase-element parameters, Electrochimica Acta. 55 (2010) 6218–6227. https://doi.org/10.1016/j.electacta.2009.10.065.

[3] P. Gong, R. Levicky, DNA surface hybridization regimes, Proceedings of the National Academy of Sciences. 105 (2008) 5301–5306. https://doi.org/10.1073/pnas.0709416105.

[4] J. Ryl, A. Zielinski, R. Bogdanowicz, K. Darowicki, Heterogeneous distribution of surface electrochemical activity in polycrystalline highly boron-doped diamond electrodes under deep anodic polarization, Electrochemistry Communications. 83 (2017) 41–45. https://doi.org/10.1016/j.elecom.2017.08.019.

[5] H.V. Patten, K.E. Meadows, L.A. Hutton, J.G. Iacobini, D. Battistel, K. McKelvey, A.W. Colburn, M.E. Newton, J.V. Macpherson, P.R. Unwin, Electrochemical Mapping Reveals Direct Correlation between Heterogeneous Electron-Transfer Kinetics and Local Density of States in Diamond Electrodes, Angew. Chem. Int. Ed. 51 (2012) 7002–7006. https://doi.org/10.1002/anie.201203057.

[6] S. Vogt, Q. Su, C. Gutiérrez-Sánchez, G. Nöll, Critical View on Electrochemical Impedance Spectroscopy Using the Ferri/Ferrocyanide Redox Couple at Gold Electrodes, Anal. Chem. 88 (2016) 4383–4390. https://doi.org/10.1021/acs.analchem.5b04814.

[7] S. Grützke, S. Abdali, W. Schuhmann, M. Gebala, Detection of DNA hybridization using electrochemical impedance spectroscopy and surface enhanced Raman scattering, Electrochemistry Communications. 19 (2012) 59–62. https://doi.org/10.1016/j.elecom.2012.03.026.

[8] P. Niedziałkowski, W. Białobrzeska, D. Burnat, P. Sezemsky, V. Stranak, H. Wulff, T. Ossowski, R. Bogdanowicz, M. Koba, M. Śmietana, Electrochemical performance of indium-tin-oxide-coated lossy-mode resonance optical fiber sensor, Sensors and Actuators B: Chemical. 301 (2019) 127043. https://doi.org/10.1016/j.snb.2019.127043.

[9] K. Silambarasan, A.V. Narendra Kumar, J. Joseph, $K_4[Fe(CN)_6]$ immobilized anion sensitive protonated amine functionalized polysilsesquioxane films for ultra-low electrochemical detection of dsDNA, Phys. Chem. Chem. Phys. 18 (2016) 7468–7474. https://doi.org/10.1039/C6CP00283H.

[10] A.A.I. Sina, L.G. Carrascosa, Z. Liang, Y.S. Grewal, A. Wardiana, M.J.A. Shiddiky, R.A. Gardiner, H. Samaratunga, M.K. Gandhi, R.J. Scott, D. Korbie, M. Trau, Epigenetically reprogrammed methylation landscape drives the DNA self-assembly and serves as a universal cancer biomarker, Nat Commun. 9 (2018) 4915. https://doi.org/10.1038/s41467-018-07214-w.